

Article

Robust Terminal Sliding Mode Control on SE(3) for Gough–Stewart Flight Simulator Motion Platform with Payload Uncertainty

Binhai Xie ^{1,2,*}  and Shuling Dai ^{1,2}

¹ The State Key Laboratory of VR Technology & Systems, Beihang University, Beijing 100191, China; sldai@buaa.edu.cn

² Jiangxi Research Institute, Beihang University, Beijing 100191, China

* Correspondence: xiebinhai@buaa.edu.cn

Abstract: This work proposes a robust terminal sliding mode control scheme on Lie group space SE(3) for Gough–Stewart flight simulator motion systems with payload uncertainty. A complete dynamic model with geometric mechanical structures and a computer dynamic model built in the MATLAB/Simulink package are briefly presented. The robust control strategy on the Lie group SE(3) is applied at the workspace level to counteract the effects of imperfect compensation due to model simplification and payload uncertainty in flight simulator application. With exponential coordinates for configuration error and adjoint operator on Lie algebra $\mathfrak{se}(3)$, the robust control strategy is designed to guarantee almost global finite-time convergence over state space through the Lyapunov stability theory. Finally, a describing function and a step acceleration response to characterize the performance of a flight simulator motion base are employed to compare the robustness performance of the proposed controller on SE(3) with the conventional terminal sliding mode controller on Cartesian space. The comparison experimental results verify that the proposed controller on SE(3) provides better robustness than the conventional controller on Cartesian space, which means higher bandwidth in two degrees of freedom and faster response with smaller tracking error in six degrees of freedom.

Keywords: robust terminal sliding mode control; exponential coordinates; Gough–Stewart platform; payload uncertainty; Lie group space SE(3)



check for updates

Citation: Xie, B.; Dai, S. Robust Terminal Sliding Mode Control on SE(3) for Gough–Stewart Flight Simulator Motion Platform with Payload Uncertainty. *Electronics* **2022**, *11*, 814. <https://doi.org/10.3390/electronics11050814>

Academic Editor: Jorge Pomares

Received: 15 January 2022

Accepted: 1 March 2022

Published: 4 March 2022

Publisher's Note: MDPI stays neutral with regard to jurisdictional claims in published maps and institutional affiliations.



Copyright: © 2022 by the authors. Licensee MDPI, Basel, Switzerland. This article is an open access article distributed under the terms and conditions of the Creative Commons Attribution (CC BY) license (<https://creativecommons.org/licenses/by/4.0/>).

1. Introduction

The Gough–Stewart (G-S) platform had been extensively employed as a motion base for flight simulators [1], which will provide high-fidelity motion cueing for pilot training when combined with a visual system and audio system in the cockpit simulator. The theoretical advantages of the parallel structure heavily depend on its motion control strategy. Although an independent PI joint controller in joint space can be applied to the G-S platform motion system, it does not always guarantee high performance due to the strong coupling and high nonlinearity of the dynamic model [2]. A cross-coupling control scheme was designed to solve the synchronization problem of the G-S platform with an adaptive feedforward gravity compensation [3].

The high level of performance has to be guaranteed through model-based control strategies on the workspace, such as inverse dynamic control, adaptive control, sliding mode control, incremental nonlinear dynamic inversion control, etc. It is well known that the inverse dynamic control strategy in [4] heavily depended on the exact modeling of the complete G-S dynamic model, which would inevitably lead to a high computational burden. Meanwhile, the study in [5] showed that the control strategy based on a simplified model provided better tracking performance than those based on a complete dynamic model.

In addition, due to the fact that the G-S motion systems suffered from parameter uncertainties and unmodeled uncertainties, more advanced model-based control strategies such

as adaptive control, robust control, and sliding mode control are necessary. The adaptive control scheme is restricted to simple parallel mechanisms [6,7] or a strongly simplified G-S dynamic model [8] due to the complicated linear form of the complete dynamic model. The robust control scheme provided another way to deal with model uncertainties and had been employed for a six-degrees-of-freedom (DOF) parallel manipulator [9,10]. The sliding mode control is another well-studied control scheme to enhance motion system robustness [11–14]. In addition, other model-based control [15], isotropic control [16], or incremental nonlinear dynamic inversion control [17] were proposed to enhance the motion tracking performance of the G-S platform.

As for control schemes designed for a six-DOF spatial rigid body, those conventional control schemes based on local motion parameterization for limited motion ranges cannot be applied to rigid body systems with large range of motion [18]. In order to model a six-DOF spatial rigid body in a geometric framework, the configuration (position and orientation) of a rigid body is represented globally on a six-dimensional special Euclidean space $SE(3)$ in a coordinate-free manner. The nonlinear control problems whose configurations are defined on Lie group space have received considerable attention in the recent literature. The early remarkable contributions from Brockett's research mainly focused on controllability issues [19]. Generally, there exist two geometric frameworks to define the configuration error on $SE(3)$. One is related to exponential coordinates on Lie group $SE(3)$ [20–22], and another one is expressed with left or right group operation between the current configuration and desired configuration [23]. Their velocity errors were calculated with the adjoint operator in its Lie algebra tangent space. With these kinematic state error vectors expressed in the Lie group and Lie algebra space, some controllers that were directly designed on $SE(3)$ were provided, and their closed-loop stability was also verified. Bullo focused on exploiting the geometric structure of Lie groups and generalizing the classical PD feedback used for the control of simple mechanical systems in \mathbb{R}^n [20,23]. With the configuration error vector based on exponential coordinates on $SE(3)$, Lee proposed a robust adaptive terminal sliding mode control strategy [24,25], while Jiang designed an asymptotic law for the spacecraft hovering over an asteroid with the second-order derivative of exponential coordinates [26]. Furthermore, Wang put forward another new configuration error function to design a geometric terminal sliding mode controller on $SE(3)$ [27].

In the flight simulator application, the contribution of its cockpit payload mounted at the upper moving platform is much more significant than the six legs in dynamic modeling of the six-DOF spatial G-S motion platform due to its limited motion envelope. Thus, the dynamic model component related with leg movement can be considered as bounded time-varying model uncertainty so as to take the control problem of the G-S platform as a control problem of the rigid body system defined on the Lie group $SE(3)$ with bounded model uncertainty. In addition, acceleration instead of positional accuracy is much more critical for flight simulation motion systems. This gives us the motivation to develop a robust terminal sliding mode controller on $SE(3)$ to provide robustness to counteract imperfect compensation due to its model simplification and payload parameter uncertainties for the flight simulator motion platform. Meanwhile, as pointed out in [10], in order to reduce the computation time, the inertial matrix and Coriolis matrix of conventional robust control law can be approximated as constants that define at the neutral point without introducing large modeling errors. Hence, the model-based robust control strategy on Cartesian space had to provide robustness to overcome this imperfect configuration-dependent model simplification uncertainty in addition to payload parameter uncertainty. However, the TSMC on Lie group $SE(3)$ does not need to consider this configuration-dependent uncertainty, as the inertial matrix of the upper platform was constant when the kinematic state is expressed in the upper moving platform-fixed coordinate. Thus, the TSMC on $SE(3)$ is expected to provide better robustness than TSMC on Cartesian space. It is designed to guarantee almost global finite-time convergence through the Lyapunov stability theory. Therefore, the main contribution of this work can be summarized as follows:

- The robust terminal sliding mode control strategy on Lie group space $SE(3)$ is applied to the G-S motion platform for the first time and has been verified to be effective in a multibody dynamic simulation environment built with the Simcape module in MATLAB/Simulink;
- When compared with conventional TSMC on Cartesian space with the model simplification scheme in [10], the proposed TSMC on $SE(3)$ with the model simplification scheme related with leg movement provides better robustness to payload uncertainty and imperfect model simplification.

The outline of this paper is listed as follows. In Section 2, a mathematical complete dynamic model of the G-S platform in geometric mechanics is derived with its kinematic state expressed in the moving platform-fixed coordinate frame. Meanwhile, a corresponding G-S computer model that was built with the Simcape module from the MATLAB/Simulink package is taken as a forward dynamic model. With exponential coordinate for configuration error and adjoint operator for velocity error, a robust terminal sliding mode controller on $SE(3)$ is designed through the Lyapunov stability analysis in Section 3. Given the description of two standard tests (the describing function, step acceleration response) and numerical experimental setup, the proposed TSMC strategy on $SE(3)$ is verified and compared with the conventional TSMC strategy on Cartesian space in Section 4. Finally, the conclusions are drawn in Section 5.

2. Dynamic Models of Gough-Stewart Platform

In this section, we will first provide a complete mathematical dynamic model of the G-S motion platform system in the body-fixed kinematic state, which preserves the geometric mechanical structure of the upper moving platform. In addition, a computer model based on the Simscape module from the MATLAB/Simulink package is built as a forward dynamic model and has been verified with its mathematical model.

The geometric structure of a general G-S motion platform is shown in Figure 1. One inertial coordinate frame $\{N\}$ is fixed on the lower fixed platform, and one body frame $\{B\}$ is fixed on the upper moving platform. Let γ denote the configuration pose of the upper moving platform, which belongs to a special Euclidean group space $SE(3) = \mathbb{R}^3 \times SO(3)$. γ can be expressed with a 4×4 homogeneous matrix as follows,

$$\gamma = \begin{bmatrix} R & p \\ 0_{1 \times 3} & 1 \end{bmatrix} \in SE(3) \quad (1)$$

Here, $p = [x, y, z]^T$ is the translational vector of geometric center O_B of the upper moving platform described in the lower fixed frame $\{N\}$. R is the orientation matrix between these two coordinate frames, which can be parameterized by three Euler angles $\Theta = [\phi, \theta, \psi]^T$ in Z-Y-X order (Yaw-Pitch-Roll). Therefore, the configuration pose γ can be locally parameterized through a six-dimensional Cartesian coordinate vector $q = [x, y, z, \phi, \theta, \psi]^T \in \mathbb{R}^6$. In order to exploit the geometric structure of the G-S dynamic model for the following controller design, we transform the Cartesian coordinate velocity \dot{q} in frame $\{N\}$ into body velocity $\xi = [\omega_B^T, v_B^T]^T$ expressed in moving platform frame $\{B\}$,

$$\xi = \begin{bmatrix} \omega_B \\ v_B \end{bmatrix} = \begin{bmatrix} R_\omega \dot{\Theta} \\ R^T \dot{p} \end{bmatrix} \in \mathbb{R}^6 \quad (2)$$

where R_ω is the transformation matrix between the body angular velocity ω_B and Euler angle derivatives $\dot{\Theta}$.

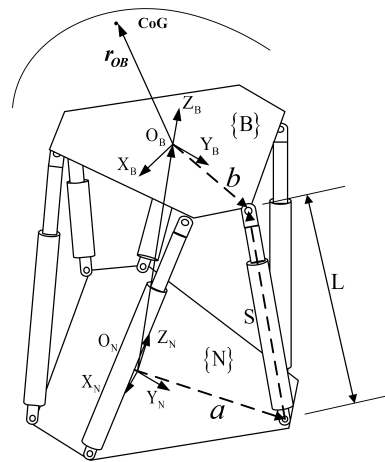


Figure 1. The geometric structure of a general G-S motion platform.

As the upper moving platform contributes to the major part of the G-S complete dynamic model, especially when the ratio of the platform to the leg is obviously large, we can derive a complete dynamic model among which we can preserve the geometric mechanics of the upper moving platform.

$$\mathbb{I}_B \dot{\zeta} = ad_{\zeta}^* \mathbb{I}_B \zeta - \varphi_{GB} - \varphi_{GL} - \varphi_{dL} + J_B^T \varphi_c \tag{3}$$

where \mathbb{I}_B denotes the inertia tensor matrix for the moving platform with payload, φ_{GB} is the gravity component vector for the moving platform payload, φ_{GL} is the gravity component of six legs, and φ_{dL} denotes the other residual component vector due to leg movement. Here, J_B denotes the kinematic Jacobian matrix with respect to new kinematic state ζ . The six-dimensional vector φ_c is the actuator force that drives the six legs.

$$\mathbb{I}_B = \begin{bmatrix} I_B & m_B \hat{r}_{OB} \\ -m_B \hat{r}_{OB} & m_B I_3 \end{bmatrix} \in \mathbb{R}^{6 \times 6}, \quad \varphi_{GB} = \begin{bmatrix} -m_B \hat{r}_{OB} R^T g \\ -m_B R^T g \end{bmatrix} \in \mathbb{R}^6 \tag{4}$$

Here, I_B is the moment of inertial parameters of the moving platform (including payload) in frame $\{B\}$, m_B is the mass parameters of the moving platform (including payload), r_{OB} is the CoG positional vector of the moving platform with its cockpit payload, which is expressed in the body-fixed frame $\{B\}$. The operator $\widehat{(\cdot)} : \mathbb{R}^3 \rightarrow so(3)$ is defined so that $\widehat{xy} = x \times y$ for all $x, y \in \mathbb{R}^3$. The vector g is the constant gravitational acceleration.

The kinematic Jacobian matrix J_B and co-adjoint operator ad_{ζ}^* are formulated as follows. The co-adjoint operator is applied to derive the dual of the Lie algebra.

$$J_B = \begin{bmatrix} (\frac{S_1}{L_1})^T R \hat{b}_1^T & (\frac{S_1}{L_1})^T R \\ \vdots & \vdots \\ (\frac{S_6}{L_6})^T R \hat{b}_6^T & (\frac{S_6}{L_6})^T R \end{bmatrix}, \quad ad_{\zeta}^* = \begin{bmatrix} -\hat{\omega}_B & -\hat{\nu}_B \\ 0_{3 \times 3} & -\hat{\omega}_B \end{bmatrix}, \tag{5}$$

where S_1, \dots, S_6 denote link vectors of six legs expressed in the lower fixed frame $\{N\}$ (see Figure 1). b_1, \dots, b_6 are the position vectors of six lower joints in the lower frame $\{N\}$, and L_1, L_2, \dots, L_6 are the lengths of six links.

In addition, we also need to construct a forward dynamic model of the G-S motion platform as a controlled system plant. As a Simscape Multibody-based dynamic model is more insensitive to the floating-point calculation error, it is chosen as the forward dynamic simulation for the G-S platform motion system instead of its mathematical model. In this work, we modify the G-S example model in the Simscape Multibody Library with our custom parameters to construct an integrated simulation environment for controller performance evaluation. The Simscape model structure for the whole G-S platform and its 3D animation is shown in the following Figures 2 and 3, respectively. Each leg model in

Figure 4 is composed of two universal joints connected to the upper and lower platform base, one extensive piston at the upper part of this leg and another one rotating cylinder at the lower part, while a two-DOF cylindrical joint connects the upper part and lower part of this leg.

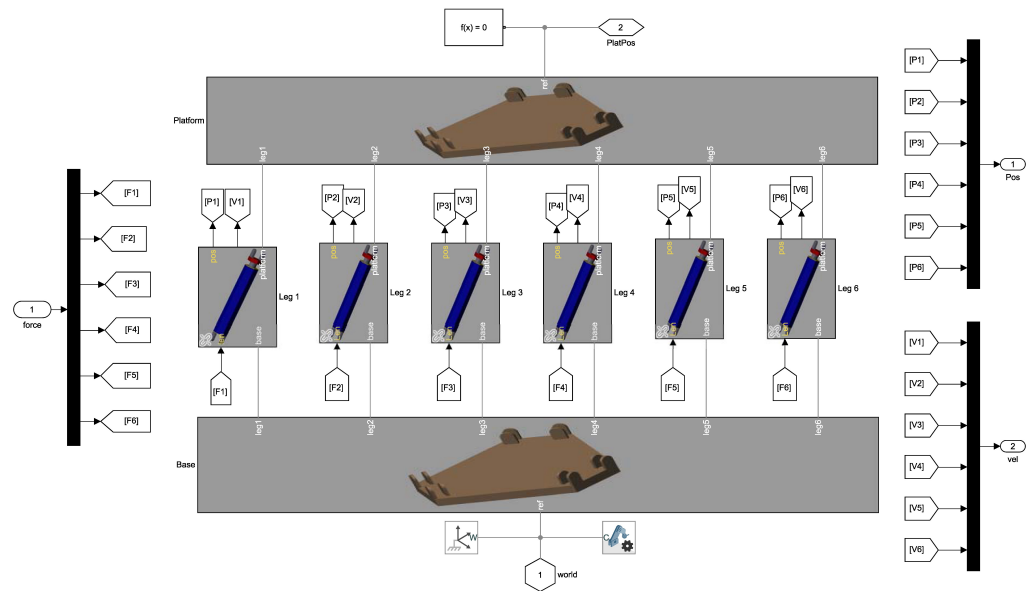


Figure 2. The Simscape model structure of a G-S platform.

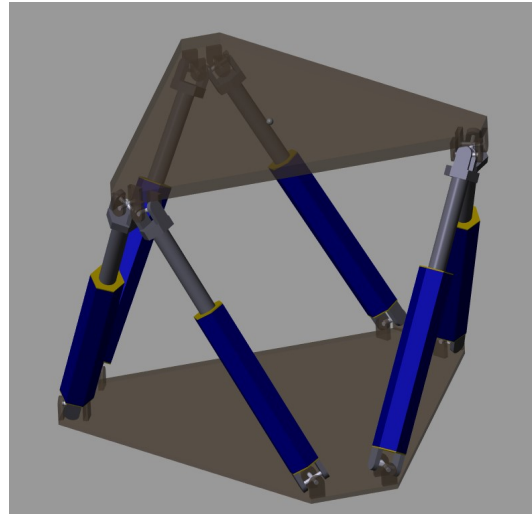


Figure 3. The 3D animation of a G-S Simscape model in Mechanics Explorer.

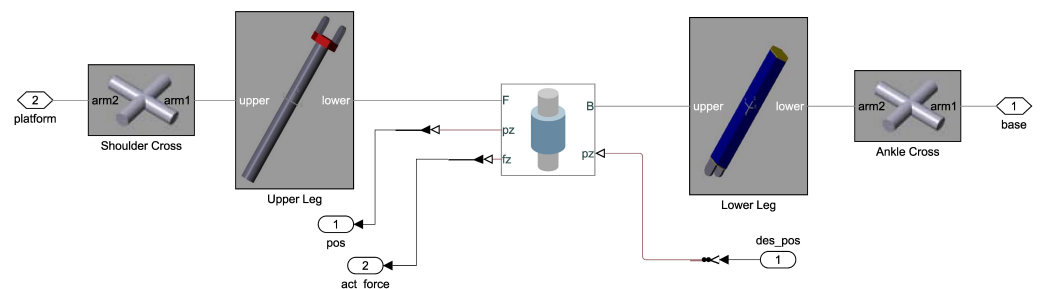


Figure 4. The Simscape model structure of one leg.

Finally, a mutual inverse dynamic model output verification experiment between the mathematical model and Simscape-based computer model had been carried out by comparing the actuator force output when given the same trajectory for these two G-S models.

3. Robust Controller Design on Lie Group Space SE(3)

Recently, Lee had provided a robust adaptive terminal sliding mode control on SE(3) in the framework of geometric mechanics for the autonomous rendezvous and docking of two spacecraft with unknown disturbances and moment of inertia uncertainty [24]. Inspired by this control scheme, we propose a TSMC strategy on SE(3) for the G-S motion platform to deal with fast-varying yet bounded model uncertainties due to model simplification as well as bounded slow-varying payload parameter variation. The control objective is to design control input such that the trajectory errors converge to zero asymptotically in finite time.

For a general G-S motion system, let $\gamma_d \in SE(3)$ be the desired configuration pose and $\gamma \in SE(3)$ be the current configuration pose. Thus, a natural configuration tracking error between γ and γ_d on Lie group space SE(3) can be defined with the right group operation as follows.

$$\gamma_e = \gamma_d^{-1}\gamma = \begin{bmatrix} R_d^T R & R_d^T (p - p_d) \\ 0 & 1 \end{bmatrix} \tag{6}$$

In this work, the configuration tracking error of the G-S platform can be further expressed in exponential coordinates using the following logarithm map,

$$\hat{\eta} = \log(\gamma_d^{-1}\gamma) \tag{7}$$

where $\log : SE(3) \rightarrow \mathfrak{se}(3)$ is the logarithm map that maps a group element in SE(3) space to Lie algebra space $\mathfrak{se}(3)$. We can regard the logarithmic map as a local chart of the manifold group SE(3) (more details can be seen in [20]). Thus, the configuration tracking error is expressed in vector form of exponential coordinates as follows,

$$\eta = \begin{bmatrix} \Psi \\ \beta \end{bmatrix} \in \mathbb{R}^6 \tag{8}$$

where $\Psi \in \mathbb{R}^3$ and $\beta \in \mathbb{R}^3$ are exponential coordinate vectors for the attitude tracking error (principal rotation vector) and position tracking error, respectively. We should notice that the logarithm map is bijective when the principal angle of rotation has a magnitude less than π radians, i.e., $\|\Psi\| < \pi$.

The velocity error ζ_e between the current velocity ζ and desired velocity ζ_d can be derived in the Lie algebra vector space as follows,

$$\zeta_e = \zeta - Ad_{\gamma_e^{-1}}\zeta_d \tag{9}$$

where Ad_g is adjoint action on SE(3) that is defined as follows,

$$Ad_g = \begin{bmatrix} R & 0_{3 \times 3} \\ \hat{p}R & R \end{bmatrix} \in \mathbb{R}^{6 \times 6}, \quad s.t. \quad Ad_g X^\vee = (gXg^{-1})^\vee \tag{10}$$

As given in reference [20], the kinematics of exponential coordinates provided the relations between η and velocity error ζ_e as follows,

$$\dot{\eta} = G(\eta)\zeta_e \tag{11}$$

The explicit expansion formulation for matrix $G(\eta)$ can be found in [20].

The time derivative of the velocity error ζ_e can be derived as follows,

$$\begin{aligned} \dot{\zeta}_e &= \dot{\zeta} - Ad_{\gamma_e^{-1}}\dot{\zeta}_d - \frac{d}{dt}(Ad_{\gamma_e^{-1}})\zeta_d \\ &= \dot{\zeta} - Ad_{\gamma_e^{-1}}\dot{\zeta}_d + [\zeta_e, Ad_{\gamma_e^{-1}}\zeta_d] \end{aligned} \tag{12}$$

where $[\cdot, \cdot] : \mathbb{R}^6 \times \mathbb{R}^6 \rightarrow \mathbb{R}^6$ is the Lie bracket operator for the Lie algebra vector (see Lie bracket definition in [28]).

Substituting the acceleration Equation (12) to the G-S platform dynamic, Equation (3) produces the following configuration error dynamic equation,

$$\mathbb{I}_B \ddot{\xi}_e = ad_{\xi}^* \mathbb{I}_B \dot{\xi} - \varphi_{GBL} - \varphi_{dL} + J_B^T \varphi_c + \mathbb{I}_B([\xi_e, Ad_{\gamma_e^{-1}} \xi_d] - Ad_{\gamma_e^{-1}} \dot{\xi}_d) \tag{13}$$

where $\varphi_{GBL} = \varphi_{GB} + \varphi_{GL}$ is a composition for the gravity component of the moving platform and legs.

In flight simulation application, the characteristic of the G-S dynamic model depends on the commanded trajectory that provides high-quality motion cues for flight training. For example, in low-frequency motion, the actuators' position and velocity constraint limit the maximal available acceleration. Moreover, the high-frequency motion keeps the moving platform not far away from its neutral position. Thus, the imperfect compensation due to model simplification also depends on its motion envelope for flight simulation.

As for the model simplification strategy, when a G-S dynamic model in Cartesian coordinate q (see reference [1]) was employed in model-based controller law for flight simulator application, the matrices $M_t(q, \dot{q})$, $C_t(q, \dot{q})$, and $G_t(q)$ need to be considered approximated as constant components with acceptable modeling errors. Under its motion envelope, the configuration pose-dependent inertial matrix for the upper moving platform with payload M_p could present 8% variation of its nominal inertial matrix at neutral pose in the low-frequency high-amplitude motion, contributing to 25% of the whole model simplification error. However, the model simplification based on dynamic model Equation (3) with configuration-independent inertial matrix \mathbb{I}_B only presents model simplification error related to leg movement. For the leg part of both of these two dynamic models, its gravity component φ_{GL} and residual component φ_{dL} can be considered as a constant vector without generating large modeling errors under the limited motion envelope.

In addition, there are always slow time-varying or unknown parameter uncertainties for the upper platform with a changeable payload due to pilot adjustment or additional equipment. Therefore, both model simplification error and payload parameter uncertainties contribute to the G-S model uncertainties boundedness in the following Assumption 1. Based on this model simplification scheme and uncertainty boundedness, the derivation of model-based robust control law becomes much simpler, which would reduce the computation time significantly.

Assumption 1. (*G-S Motion System imperfect model compensation boundedness*) *The simplified G-S dynamic model provided in Equation (3) contains imperfect model compensation from the intentional simplification of the leg component and inaccurate constant and time-varying model parameters. The generalized forces and torques corresponding to model error are assumed to be bounded. Thus, it is assumed that there exists a constant boundary vector $F = [F_1 \ F_2 \ \dots \ F_6]^T$ such that*

$$|\varphi_{dL}| = \begin{cases} |\tau_{d_i}| \leq F_j & i, j = 1, 2, 3, \\ |\phi_{d_i}| \leq F_j & i = 1, 2, 3, j = 4, 5, 6 \end{cases} \tag{14}$$

It is obvious that the G-S model uncertainty in Equation (3) does not need to deal with configuration-dependent uncertainty related to a moving platform so as to provide us with a more reasonable boundary to enhance the robustness of the control law. The sliding mode control scheme is capable of dealing with model uncertainties. It is well known that a fundamental difference in flight simulator motion systems w.r.t usual robotics is the fact that acceleration instead of positional accuracy is more important. Thus, this work is devoted to designing a robust terminal sliding mode control scheme for the G-S motion system with model uncertainties.

The terminal sliding plane on the Lie group SE(3) is defined as follows,

$$s = \xi_e + C\eta^{q/p} \tag{15}$$

where $s = [s_1 \ s_2 \ s_3 \ s_4 \ s_5 \ s_6]^T \in \mathbb{R}^6$ is the sliding plane, $\eta = [\eta_1 \ \eta_2 \ \eta_3 \ \eta_4 \ \eta_5 \ \eta_6]^T \in \mathbb{R}^6$, $C = \text{diag}(c_1, c_2, c_3, c_4, c_5, c_6)$ is a positive definite matrix, and the positive odd integers q, p are chosen such that $q > p$.

Theorem 1. For the nonlinear error kinematics and dynamics described in Equations (11) and (13), if the sliding plane is designed as Equation (15), the system motion will converge to zero along the sliding plane $s(t) = 0_{6 \times 1}$ in finite time, and the control law is designed as follows,

$$\varphi_c = -J_B^{-T} (ad_{\xi}^* \mathbb{I}_B \xi - \varphi_{GBL} + \mathbb{I}_B([\xi_e, Ad_{\gamma_e^{-1}} \xi_d] - Ad_{\gamma_e^{-1}} \dot{\xi}_d + \Lambda G(\eta) \xi_e) + K \text{sat}(s, \epsilon)) \quad (16)$$

where $\Lambda = \text{diag}(\frac{c_1 q}{p} \eta_1^{q/p-1}, \frac{c_2 q}{p} \eta_2^{q/p-1}, \dots, \frac{c_6 q}{p} \eta_6^{q/p-1})$, $\text{sat}(s, \epsilon) = [\text{sat}(s_1, \epsilon), \text{sat}(s_1, \epsilon), \dots, \text{sat}(s_6, \epsilon)]^T$ are saturation functions, and $K = \text{diag}(k_1, k_2, \dots, k_6)$ is a positive definite gain matrix satisfying the following inequality,

$$k_i > F_i, \quad i = 1, 2, \dots, 6 \quad (17)$$

Proof. Consider the following Laypunov function candidate,

$$V = \frac{1}{2} s^T \mathbb{I}_B s \quad (18)$$

Taking the time derivative of the Laypunov function V results in,

$$\dot{V} = s^T \mathbb{I}_B (\dot{\xi}_e + C \dot{\eta}^{\frac{q}{p}}) \quad (19)$$

Substituting the error dynamic Equation (13) and kinematic Equation (11) into Equation (19), the derivative will be written as,

$$\dot{V} = s^T [ad_{\xi}^* \mathbb{I}_B \xi - \varphi_{GBL} + J_B^T \varphi_c + \varphi_{dL} + \mathbb{I}_B([\xi_e, Ad_{\gamma_e^{-1}} \xi_d] - Ad_{\gamma_e^{-1}} \dot{\xi}_d + \Lambda G(\eta) \xi_e)] \quad (20)$$

Finally, taking the control law Equation (16) into Equation (20) yields the following equation.

$$\dot{V} = s^T [\varphi_{dL} - K \text{sat}(s, \epsilon)] \leq - \sum_{i=1}^6 (k_i |s_i| - F_i |s_i|) = - \sqrt{\frac{2}{\lambda_{\min}(\mathbb{I}_B)}} \rho V^{\frac{1}{2}} \quad (21)$$

where $\rho > 0$ and $\lambda_{\min}(\mathbb{I}_B)$ is the minimum eigenvalue of inertia matrix \mathbb{I}_B . Therefore, through the finite-time stability theorem in [29], we can draw the conclusion that the G-S platform kinematic state will reach the sliding surface $s(t) = 0_{6 \times 1}$ in finite time. The closed-loop system under control law (16) will globally stabilize $(\eta, \xi_e) = (0_{6 \times 1}, 0_{6 \times 1})$ in finite time. \square

Remark 1. As mentioned in [30], in order to avoid the possible singularity problem in the TSMC as η converges to zero, the parameters p and q are properly chosen so that $2q > p$.

The controller framework for the G-S motion system is shown in Figure 5. Those six legs are actuated through a PMSM drive modeled through a simplified transfer function as clarified in reference [12], and it can meet the controller demand output with a current loop bandwidth over 100 Hz in torque control mode. The forward kinematics of the G-S platform can be computed in real time by employing a Newton–Raphson method.

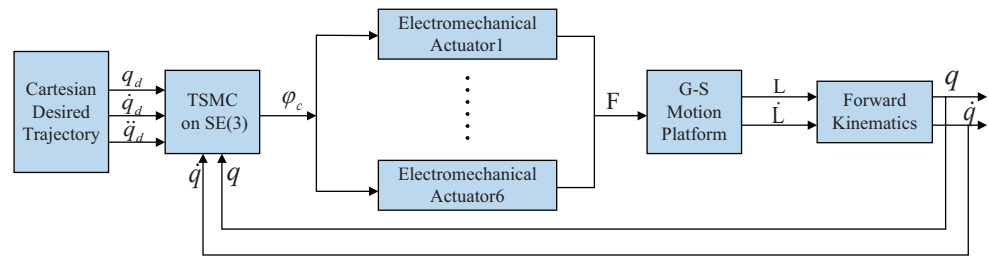


Figure 5. The control framework of TSMC on SE(3) for G-S motion systems.

4. Controller Performance Evaluation and Analysis

This section is devoted to evaluating the robustness performance of the TSMC strategy on SE(3) through a comparison with the conventional TSMC strategy on Cartesian space in a G-S motion platform simulated testbed. The main parameters of the G-S motion system are shown in Tables 1 and 2. In this work, two standard methods from the AGARD report 144 [31] are considered: the describing function test for frequency domain evaluation and the step acceleration response for time domain evaluation. For each degree of freedom, six describing functions can be calculated at operating points in the following Table 3. The primary describing function is the comparison of the response of motion base in the driven DOF to the excitation signal. The amplitudes of sinusoidal input were chosen to keep the motion below approximately 10% of the system limits in position, velocity, and acceleration. The amplitude of the step acceleration input is chosen to be 70% of the system limits. The simulation step size is chosen to be 0.01 ms, and the ODE45 solver is used.

Table 1. Mass and inertial parameters of the G-S platform.

Parameters	Description	Values
m_B	Mass of moving platform	2600 kg
I_B	Inertial matrix of moving platform	$diag\{2716, 2716, 3800\} \text{kg} \cdot \text{m}^2$
r_{OB}	CoG of moving platform	[0,0,0.40] m
m_u	Mass of upper piston of each leg	78 kg
m_d	Mass of lower cylinder of each leg	148 kg
d_u	CoG of piston in its local frame	[0.82,0,0] m
d_d	CoG of cylinder in its local frame	[0.86,0,0] m
I_u	Inertial of piston with respect to local frame	$diag\{0.26, 18.53, 18.53\} \text{kg} \cdot \text{m}^2$
I_d	Inertial of cylinder with respect to local frame	$diag\{1.189, 28.09, 28.09\} \text{kg} \cdot \text{m}^2$
g	Gravitational acceleration	9.8066 m/s ²

Table 2. The geometric parameters of the G-S platform.

Parameters	Description	Values
r_B	The upper moving platform radius	1.60 m
r_N	The lower fixed platform radius	1.65 m
d_B	Upper platform spacing	0.1 m
d_N	Lower platform spacing	0.3 m
L_{min}	Minimum leg length	1.8 m
L_{max}	Maximum leg length	2.6 m

Table 3. Operating points for describing function tests.

Sinusoidal Acceleration for Translation		Sinusoidal Velocity for Rotation	
Freq (Hz)	Amp (m/s ²)	Freq (Hz)	Amp (rad/s)
0.3	0.1	0.3	0.020
0.5	0.5	0.5	0.016
0.8	0.5	0.8	0.016
1.3	0.5	1.3	0.012
2.0	0.5	2.0	0.012
3.2	0.5	3.2	0.010
5.0	0.5	5.0	0.008
7.1	0.5	7.1	0.006
9.1	1.0	9.1	0.006
10.1	1.0	10.1	0.006
11	1.0	11	0.006
13	1.0	13	0.006
14.8	1.0	14.8	0.006
19.8	0.15	19.8	0.002

For the Simscape-based G-S platform model plant, the parameter uncertainties of its moving platform payload are set with the following equations.

$$\begin{aligned}
 \Delta m &= (0.07 + 0.01\sin(0.1t)) \cdot m \\
 \Delta r_{OB} &= (0.06 + 0.02\sin(0.2t)) \cdot r_{OB} \\
 \Delta I_B &= (0.06 + 0.02\sin(0.2t)) \cdot I_B
 \end{aligned} \tag{22}$$

These payload parameter uncertainty equations show that the actual payload parameters vary in the range of 6–8% of its nominal values, which include a constant uncertainty and a slow time-varying uncertainty. With the known dynamic model simplification characteristic of G-S dynamics under a limited motion envelope, it is easy to determine a conservative boundary vector for a flight simulator motion system. Therefore, the controller parameters for TSMC on SE(3) are set as shown in Table 4.

Table 4. The controller parameters for TSMC on SE(3).

Controller Parameters	Values
p, q	$p = 3, q = 5$
C	$\begin{bmatrix} 0.758I_3 & 0 \\ 0 & 0.842I_3 \end{bmatrix}$
K	$diag\{600, 500, 560, 400, 400, 2700\}$
ϵ	0.003

After the description of the test procedure and experimental setup, the amplitude and phase frequency characteristics of the closed-loop G-S motion system under the TSMC controller law on SE(3) from 0.3 to 20 Hz are shown in Figures 6 and 7. Meanwhile, given the same describing function test and experimental setup, a TSMC strategy in Cartesian space provides the amplitude and phase frequency characteristics in the following Figures 8 and 9.

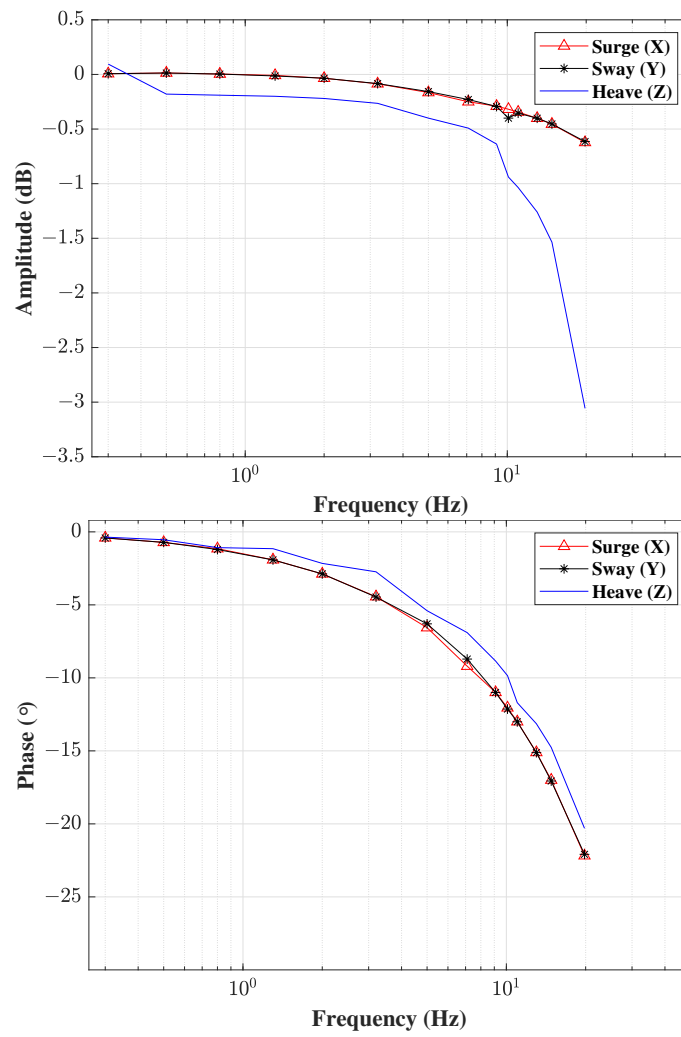


Figure 6. The Bode plot for a translational describing function under TSMC on SE(3).

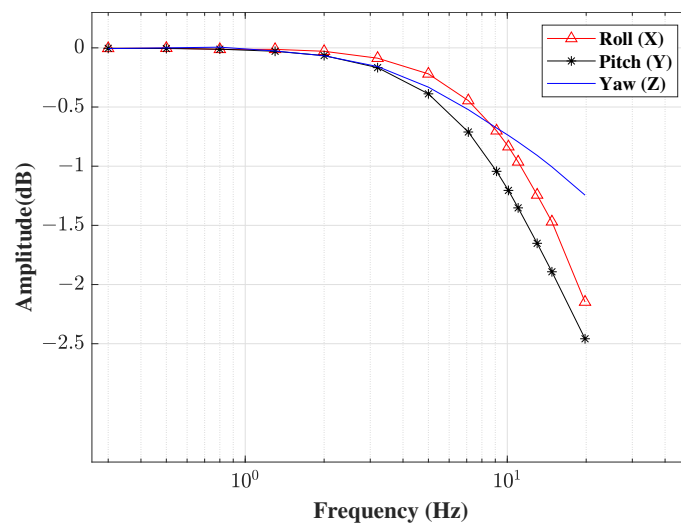


Figure 7. Cont.

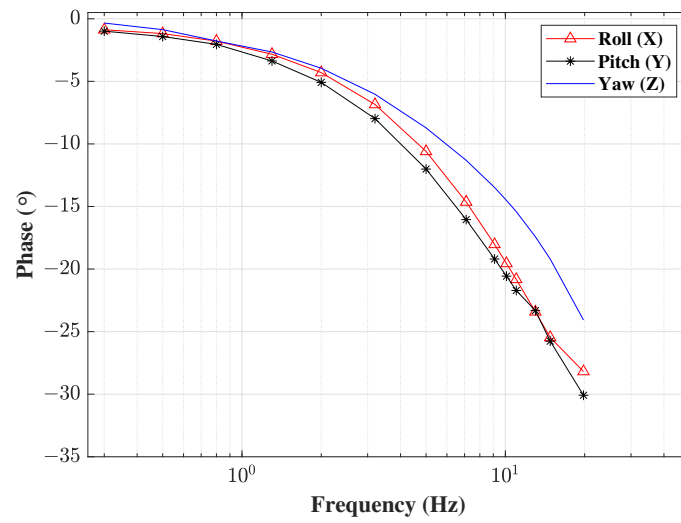


Figure 7. The Bode plot for a rotational describing function under TSMC on SE(3).

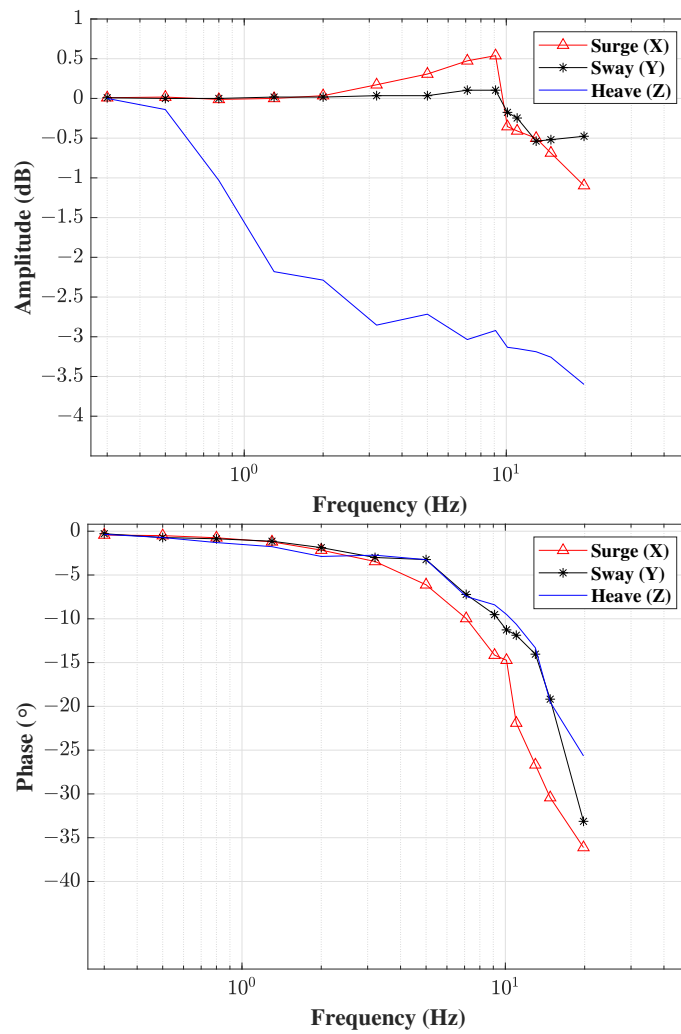


Figure 8. The Bode plot for a translational describing function under TSMC on Cartesian space.

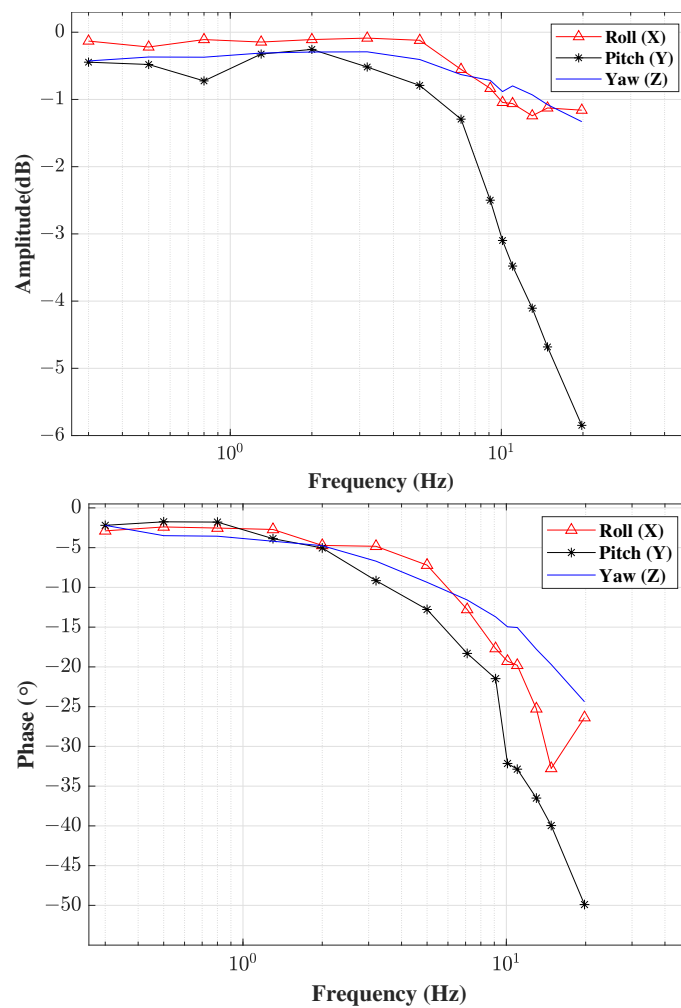


Figure 9. The Bode plot for a rotational describing function under TSMC on Cartesian space.

For the TSMC strategy on SE(3), it can be seen that the systems presented a flat response with a bandwidth of approximately 20 Hz in the surge, sway, roll, pitch, and yaw directions. Meanwhile, the -3 dB point of heave direction can be found around 13 Hz. In all six DOFs, the phase lag remains well within 45° . However, for the TSMC strategy on Cartesian space, it is only in the surge, sway, roll, and yaw directions that the bandwidth can arrive at 20 Hz. In the heave direction, the -3 dB point has dropped to 7.1 Hz. In the pitch direction, the -3 dB point also falls to below 10 Hz, and the phase lag has exceeded 45° around 15 Hz. Thus, we can draw the conclusion that the TSMC strategy on SE(3) provides better robustness with high bandwidth in two DOFs more than TSMC on Cartesian space.

Furthermore, given another set of controller parameters for the step acceleration response test ($K = \text{diag}\{950, 950, 650, 500, 500, 4000\}$, $\epsilon = 0.007$, other parameters remain unchanged), the rise time comparisons in six DOFs are shown in Table 5. This comparison shows that the TSMC on SE(3) represents a relatively faster step response than TSMC on Cartesian space in all six DOFs, especially in the roll and yaw direction. The acceleration step responses in the roll and yaw direction are shown in the following Figures 10 and 11, respectively. It tells us that the TSMC on SE(3) also behaves with smaller acceleration tracking error than TSMC on Cartesian space. This is due to the fact that the TSMC strategy had to cost much more robustness in dealing with its configuration-dependent model simplification error in the high-amplitude rotation motion.

Table 5. The rise time comparison for TSMC on SE(3) and Cartesian space.

DOF	TSMC on SE(3)	TSMC on Cartesian Space
x	12.40 ms	14.40 ms
y	12.30 ms	14.60 ms
z	12.00 ms	12.10 ms
ϕ	17.17 ms	23.80 ms
θ	17.33 ms	23.50 ms
ψ	14.66 ms	15.10 ms

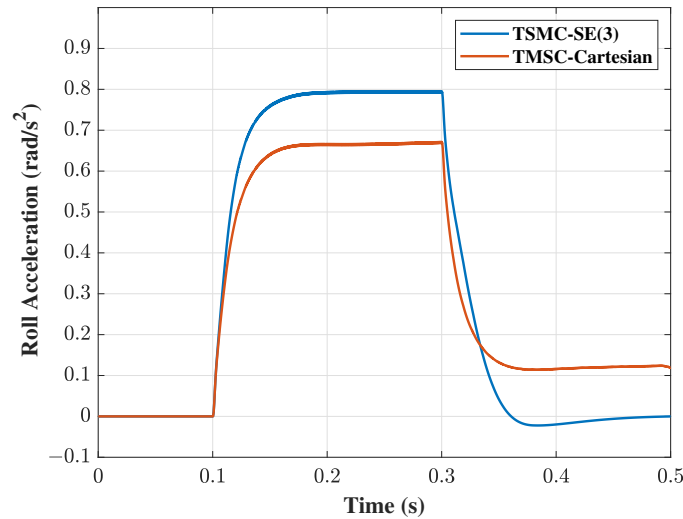


Figure 10. The step acceleration response comparison in the roll direction.

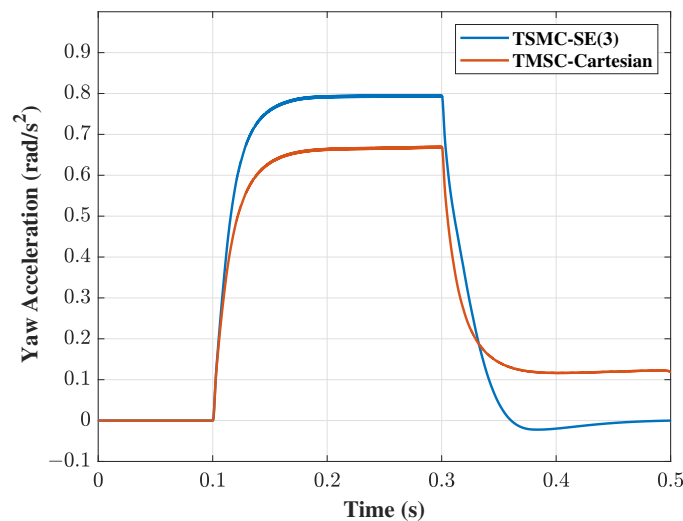


Figure 11. The step acceleration response comparison in the yaw direction.

As stated by Koekebakker [1], the controlled simulator motion system requires a bandwidth over 10 Hz so as to have minimal influence on the pilot–aircraft model loop characteristics. Through the performance comparison in the frequency-domain and time-domain, we can conclude that the TSMC strategy on SE(3) would be beneficial for robust controller design for a flight simulator motion base. In addition, it should be noticed that the frequency-domain and time-domain performance of the controlled system would worsen in physical implementation due to the increased response time of inner-loop PMSM drive systems.

5. Conclusions

This paper proposed a robust terminal sliding mode controller on SE(3) for a G-S flight simulator motion system with payload uncertainty. A simplified dynamic model that preserved the geometric mechanical structure of the major moving platform under the limit motion envelope was provided. The robust strategy worked in the out-loop workspace to deal with the imperfect model compensation due to model simplification and payload uncertainty. Within the Lyapunov stability framework, the designed robust control scheme was proven to guarantee finite-time convergence. Finally, a standard describing function test for the frequency-domain and a step acceleration response for the time-domain were used to compare the robustness performance of the TSMC strategy on SE(3) with TSMC strategy on Cartesian space. The experimental results showed that the TSMC strategy on SE(3) provided better robustness than the conventional TSMC strategy on Cartesian space: that is, higher bandwidth in two DOFs and relatively faster response with smaller acceleration tracking error in the time-domain. In future study, we will finish the inner-loop PMSM dynamic model with a Simscape Electrical module in MATLAB/Simulink instead of the current transfer function model so as to make the simulated testbed closer to the physical environment. In addition, we will continue to perform other standard tests in the AGARD report for the proposed TSMC strategy before the real-life application.

Author Contributions: Conceptualization, B.X. and S.D.; methodology, B.X.; software, B.X.; validation, B.X. and S.D.; investigation, B.X.; writing—original draft preparation, B.X.; writing—review and editing, S.D.; visualization, B.X.; supervision, S.D.; project administration, S.D. All authors have read and agreed to the published version of the manuscript.

Funding: This research is funded by the National Key Research and Development Plan of China (No.2018AAA0102902).

Institutional Review Board Statement: Not applicable.

Informed Consent Statement: Not applicable.

Data Availability Statement: Not applicable.

Acknowledgments: Not applicable.

Conflicts of Interest: The authors declare no conflict of interest.

Abbreviations

The following abbreviations are used in this manuscript:

G-S	Gough–Stewart
DOF	Degree of Freedom
CoG	Center of Gravity
TSMC	Terminal Sliding Mode Controller
PMSM	Permanent magnet Synchronous Motor
AGARD	Advisory Group for Aerospace Research & Development

References

1. Koekebakker, S.H. Model Based Control of a Flight Simulator Motion System. Ph.D. Thesis, Delft University of Technology, Delft, The Netherlands, 2001.
2. Paccot, F.; Andreff, N.; Martinet, P. A review on the dynamic control of parallel kinematic machine: Theory and Experiments. *Int. J. Robot. Res.* **2009**, *28*, 395–416. [[CrossRef](#)]
3. Zhao, D.; Li, S.; Gao, F. Fully Adaptive Feedforward Feedback Synchronized Tracking Control for Stewart Platform Systems. *Int. J. Control. Autom. Syst.* **2008**, *6*, 689–701.
4. Lee, S.H.; Song, J.; Choi, W.; Hong, D. Position control of a Stewart platform using inverse dynamics control with approximate dynamics. *Mechatronics* **2003**, *13*, 605–619. [[CrossRef](#)]
5. Daiz-Rodriguez, M.; Valera, A.; Mata, V.; Valles, M. Model-based control of a 3-DOF parallel robot based on identified relevant parameters. *IEEE/ASME Trans. Mechatronics* **2013**, *18*, 1737–1744. [[CrossRef](#)]

6. Shang, W.; Cong, S.; Ge, Y. Adaptive computed torque control for a parallel manipulator with redundant actuation. *Robotica* **2011**, *30*, 457–466. [[CrossRef](#)]
7. Ren, L.; Mills, J.; Sun, D. Experimental Comparison of Control Approaches on Trajectory Tracking Control of a 3-DOF parallel robot. *IEEE Trans. Control Syst. Technol.* **2007**, *15*, 982–988. [[CrossRef](#)]
8. Wu, D.; Gu, H. Adaptive sliding control of six-DOF flight simulator motion platform. *Chin. J. Aeronaut.* **2007**, *20*, 425–433.
9. Kim, H.; Cho, Y.; Lee, K. Robust nonlinear task space control for a 6 DOF parallel manipulator. *Automatica* **2005**, *41*, 1591–1600. [[CrossRef](#)]
10. Becerra-Vargas, M.; Belo, E. Robust control of flight simulator motion base. *J. Guid. Control Dynamics* **2011**, *34*, 1519–1528. [[CrossRef](#)]
11. Guo, H.; Liu, Y.; Liu, G.; Li, H. Cascade control of a hydraulically driven 6-DOF parallel robot manipulator based on a sliding model. *Control Eng. Pract.* **2008**, *16*, 1055–1068. [[CrossRef](#)]
12. Meng, Q.; Zhang, T.; Gao, X.; Song, J. Adaptive sliding model fault-tolerant control of the uncertain Stewart platform based on offline multibody dynamics. *IEEE/ASME Trans. Mechatronics* **2014**, *19*, 882–894. [[CrossRef](#)]
13. Velasco, J.; Calvo, I.; Barambones, O.; Venegas, P.; Napole, C. Experimental validation of a sliding mode control for a Stewart platform used in aerospace inspection applications. *Mathematics* **2020**, *8*, 2051. [[CrossRef](#)]
14. Cai, Y.; Zheng, S.; Liu, W.; Qu, Z.; Zhu, J.; Han, J. Sliding-mode control of ship-mounted Stewart platforms for wave compensation using velocity feedforward. *Ocean Eng.* **2021**, *236*, 109477. [[CrossRef](#)]
15. Davliakos, I.; Papadopoulos, E. Impedance model-based control for an electrohydraulic Stewart platform. *Eur. J. Control* **2009**, *15*, 560–577. [[CrossRef](#)]
16. Yang, X.; Wu, H.; Li, Y.; Kang, S.; Chen, B.; Lu, H.; Lee, C.M.; Ji, P. Dynamics and Isotropic control of parallel mechanisms for vibration isolation. *IEEE/ASME Trans. Mechatronics* **2020**, *25*, 2027–2034. [[CrossRef](#)]
17. Huang, Y.; Pool, D.; Stroosma, O.; Chu, Q. Robust incremental nonlinear dynamic inversion controller of hexapod flight simulator motion system. In *Advances in Aerospace Guidance, Navigation and Control*; Dolega, B., Glebocki, R., Kordos, D., Zuga, M., Eds.; Springer: Heidelberg/Berlin, Germany, 2018; pp. 87–99.
18. Schaub, H.; Junkins, J. *Analytical Mechanics of Space Systems*; AIAA: Reston, VA, USA, 2003; ISBN 978-1-56347-563-4.
19. Brockett, R. The early days of geometric nonlinear control. *Automatica* **2014**, *50*, 2203–2224. [[CrossRef](#)]
20. Bullo, F.; Murray, R. Proportional derivative (PD) control on the Euclidean Group. In Proceedings of the 1995 European Control Conference, Rome, Italy, 5–8 September 1995; Volume 2, pp. 1091–1097.
21. Arabi, E.; Sarsilmaz, S.B.; Yucelen, T.; Maadani, M.; Butcher, E.A.; Nazari, M. Adaptive control of a rigid body vehicle on exponential coordinates with guaranteed performance. In Proceedings of the 2018 AIAA Guidance, Navigation, and Control Conference, Kissimmee, FL, USA, 8–12 January 2018.
22. Gong, K.; Liao, Y.; Wang, Y. Adaptive fixed-time terminal sliding mode control on SE(3) for coupled spacecraft tracking maneuver. *Int. J. Aerosp. Eng.* **2020**, *2020*, 1–15. [[CrossRef](#)]
23. Bullo, F.; Murray, R. Tracking for fully actuated mechanical systems: A geometric framework. *Automatica* **1999**, *35*, 17–34. [[CrossRef](#)]
24. Lee, D.; Vukovich, G. Robust adaptive terminal sliding mode control on SE(3) for autonomous spacecraft rendezvous and docking. *Nonlinear Dyn.* **2016**, *83*, 2263–2279. [[CrossRef](#)]
25. Lee, D.; Vukovich, G. Adaptive finite-time control for spacecraft hovering over an asteroid. *IEEE Trans. Aerosp. Electron. Syst.* **2016**, *52*, 1183–1196. [[CrossRef](#)]
26. Jiang, L.; Wang, Y.; Xu, S. Integrated 6-DOF orbit-attitude dynamical modeling and control using geometric mechanics. *Int. J. Aerosp. Eng.* **2017**, *2017*, 1–13. [[CrossRef](#)]
27. Wang, Y.; Hong, H.; Guo, J.; Wang, X.; Shang, W. Configuration error function design and application to fixed-time geometric terminal sliding-mode control on SE(3). *Acta Astronaut.* **2020**, *174*, 61–71. [[CrossRef](#)]
28. Murray, M.R.; Sastry, S.S.; Li, Z. *A Mathematical Introduction to Robotic Manipulation*; CRC Press: Boca Raton, FL, USA, 1994.
29. Bhat, S.P.; Bernstein, D.S. Finite-time stability of continuous autonomous systems. *SIAM J. Control Optim.* **2000**, *38*, 751–766. [[CrossRef](#)]
30. Hui, L.; Li, J. Terminal sliding mode control for spacecraft formation flying. *IEEE Trans. Aerosp. Electron. Syst.* **2009**, *45*, 835–846. [[CrossRef](#)]
31. Lean, D. *Dynamic Characteristics of Flight Simulation Motion Systems*; Technical Editing and Reproduction, Ltd.: London, UK, 1979; AGARD Advisory Report No. 144.